



Asymmetric effect of static radial eccentricity on the vibration characteristics of the rotor system of permanent magnet synchronous motors in electric vehicles

Feng Liu · Changle Xiang · Hui Liu ·
Lijin Han · Yunhao Wu · Xiaojie Wang ·
Pu Gao

Received: 30 December 2017 / Accepted: 6 April 2019 / Published online: 20 April 2019
© Springer Nature B.V. 2019

Abstract Considering static radial eccentricity, a Jeffcott rotor model is established for the rotor system of the permanent magnet synchronous motors in electric vehicles. The system conservative force, including unbalanced magnetic pull, which results in nonlinearity is analyzed, and center manifold theorem and Lyapunov method are used to determine the stabilities of multiple equilibrium points. This analysis shows that static eccentricity spoils the symmetry of the equilibrium points, although they are distributed in the line along the direction of the static eccentricity. This asymmetry leads to the pitchfork bifurcation of equilibrium points to a generic bifurcation with a defect. This analysis provides two stability conditions for the rotor system. Furthermore, the effect of the asymmetry on the dynamic characteristics that can induce backward whirling motion coupled with forward whirling motion is quite different from the case without static eccentricity. These characteristics are investigated by multi-scale method. As a result, the analytical solution of the system at steady state is obtained. The frequency

characteristics of the main resonance are analyzed, and the stability of the solution is determined using Routh–Hurwitz criterion and the geometric constraint of the rotor whirling motion. The characteristics reveal that a globally unstable frequency band appears due to the geometric constraint. However, this frequency band narrows and even vanishes with increases in damping and electromagnetic stiffness and decreases in mass imbalance, mechanical stiffness and static eccentricity. The analysis by multi-scale method is based on the assumption of the time invariance of the forward and backward whirling amplitudes, which is validated by the numerical method. The results of the two methods agree well, which indicates that this assumption and the analysis are reasonable.

Keywords Static eccentricity · Unbalanced magnetic pull · Static characteristics · Frequency characteristics · Stability

F. Liu · C. Xiang (✉) · H. Liu (✉) · L. Han · Y. Wu ·
X. Wang · P. Gao
School of Mechanical Engineering, Beijing Institute of
Technology, Beijing 100081, China
e-mail: xiang_changle@163.com

H. Liu
e-mail: liuhui_bit@163.com

F. Liu
Department of Mechanical Engineering, Academy of Armored
Force Engineering, Beijing 100072, China

1 Introduction

Permanent magnet synchronous motors (PMSMs) have many advantages and have been broadly applied to electric vehicles (EVs) and hybrid electric vehicles (HEVs). However, the dynamics problems of PMSMs in EVs and HEVs caused by rotor eccentricity have seriously affected machine performance. The transmission systems of the vehicles are susceptible to excessive

vibration and noise. Therefore, these problems should be investigated for suppressing vibration and noise.

For the rotating electrical machines, the radial electromagnetic forces are balanced when the rotor is concentric with the stator. However, in a practical system, rotor eccentricity appears for several reasons, such as manufacturing error, assembly error and bearing wear [1–3]. This results in unbalanced magnetic pull (UMP), which compels the rotor to deviate from the stator and has the same direction that the eccentricity. Therefore, UMP reveals a negative stiffness effect, which causes problems of dynamics in the system. To date, investigations of rotor eccentricity can be classified into three areas: UMP, detection of rotor eccentricity, and vibration generation [4].

In the past several decades, many scholars have used finite element method (FEM) and analytical method for the calculation of UMP. The former [5–12] can offer accurate solutions but cannot provide an insight into the system parameters [2]. The analysis of the dynamic characteristics of the rotor system requires the analytical expression of UMP. Therefore, an extensive approach was widely applied to the analytical calculation of UMP, which used the air-gap permeance to modulate the magnetic motive force (MMF) to obtain the air-gap flux density, which includes the eccentricity information [13–15]. Then, UMP varying with pole-pair number can be analytically carried out by Maxwell tensor method [14]. This calculation reveals that UMP is a nonlinear function with respect to the eccentricity between the stator and rotor. However, we cannot recognize the type of rotor eccentricity according to UMP.

In fact, there exist three types of rotor eccentricity: dynamic eccentricity, static eccentricity and mixed eccentricity [16, 17]. The different types of rotor eccentricity result in different patterns of system parameters such as stator current, voltage and torque. According to these patterns, many scholars employed signal processing and mathematical algorithms to detect rotor eccentricities [18–20]. Roux et al. [21] investigated the experimental implementation and detection of rotor eccentricities in PMSMs by measuring only the stator current and voltage. Ebrahimi et al. [22–25] addressed an index of noninvasive diagnosis according to the sideband of the spectrum of the stator current, torque and magnetic field analysis for the three types of eccentricity in PMSMs. Akar et al. [26] proposed a spectral analysis method to detect static eccentric-

ity fault for PMSMs and then considered the sideband effects in the vicinity of the fundamental frequency as the most important indicator of eccentricity. In reference [27], then they detected static eccentricity through a probability distribution based on equal width discretization and a neural network model. Mirimani et al. [28] used 3-D finite element analysis to study the detection of static eccentricity for permanent magnet machines, validated this numerical model by experimental measurements, presented an appropriate criterion for eccentricity detection by the back electromotive force and developed an online method for static eccentricity fault detection [29]. Hong et al. [30] presented a technique for automated monitoring of air-gap eccentricity, which was to use the inverter for testing of PMSMs at motor standstill. Da et al. [31] used direct flux measurement to develop an index of multi-fault detection in PMSMs that can determine the direction of static eccentricity. Karami et al. [32] employed an analysis of the performance of a line start PMSM with static eccentricity in steady state by FEM. Huang et al. [33] calculated the static eccentricity of a double rotor axial flux permanent magnet machine by an analytical model whose results were verified via experiment. Goktas et al. [34] addressed the discernment of static eccentricity and broken magnet faults in PMSMs through the stator phase current due to their strongly similar fault patterns in the back electromotive force and flux spectrum. Naderi et al. [35] studied the eccentricity fault by the current/torque signature and recognized the static and dynamic eccentricity faults by the power spectral density of the vibration signal and stator current. Naderi [36] further addressed a torque ripple analysis for four separate synchronous reluctance machines under health and eccentricity fault conditions considering slot opening and distributed winding effects. Oumaamar et al. [37] presented an alternative method based on the analysis of line neutral voltage for static eccentricity detection. Most of these references covered the detection of static eccentricity, which is a vital consideration for the fault diagnosis of electric machines. However, these papers did not focus on the dynamics mechanism caused by static eccentricity, which can provide the dynamical criterion of the detection. In fact, static eccentricity can also be susceptible to some dynamics problems such as excessive vibration and loss of stability, which are important considerations for the dynamic system. These dynamic effects can result in fault patterns that carry information about

the type and degree of rotor eccentricity. Therefore, an investigation of the dynamic characteristics should be considered, which can provide insight to the eccentricity fault diagnosis and accurate detection.

UMP caused by rotor eccentricity exhibits a negative stiffness effect and nonlinearity, which play a key role in dynamic behaviors. Cylindrical and conical whirls induced by mass imbalance and external forces result in rotor eccentricity and hence UMP compelling the rotor to further move toward the stator and then distort the air-gap distribution [2]. This is a typical electromechanical coupling system [38] in which dynamic behaviors have been investigated in many papers. Pennacchi et al. [1] presented a vibration analysis for a generator considering the external exciting forces, including the mass imbalance of the rotor and the effect of UMP. He et al. [39] built up the finite element and boundary element models of a motor considering static eccentricity to predict the modal parameters, the dynamic vibrations, and the sound pressures. Shin et al. [40] employed the finite element analysis method to estimate the vibration characteristics of PMSMs. Xu et al. [41] took advantage of FEM to predict the vibration influenced by UMP. The results show that static eccentricity will lead to an offset in the axis center and give rise to the nonlinearity of the dynamic response. FEM can obtain accurate results but cannot provide insight into the dynamics mechanism of the rotor system. Kim et al. [38] analyzed the transient whirl response of a rotor system considering mass imbalance by a finite element-transfer matrix, and the computational efficiency is higher than that of FEM. This investigation shows that UMP reduces the system stiffness, which leads to more serious vibration compared with that of purely mechanical origins. The negative stiffness effect of UMP causes the stability problem, which has attracted the attention of scholars. Calleecharan et al. [16] applied the Jeffcott rotor model to the generator, performed a vibration analysis and noted the static eccentricity resulting in a decrease in the stability and even a loss of stability. Wu et al. [42] developed a four degrees of freedom rotor model considering the gyroscopic effect and investigated the dynamic behavior and stability of the generator. Lundström et al. [43] analyzed the dynamic response of the generator considering the shape deviations of the rotor and investigated the attraction basins for contact between the rotor and stator. Xiang et al. [44] investigated multiple equilibrium points and their stabilities by Lyapunov direct method and analyzed the free

vibration and frequency characteristics of the rotor of the PMSMs used in EVs. This study discovered the coupling mechanism of the modulation effect of radial displacement components. However, the influence of static eccentricity was neglected in references [42–44]. Xu et al. [45] focused on the nonlinear vibration of a rotor with static and dynamic eccentricities. The vibration characteristics were discussed in detail for comparison. However, the analyses were performed by numerical method.

As mentioned above, the investigations of static eccentricity were mainly restricted to detection and diagnosis. In addition, a portion of the papers focusing on the rotor dynamics of electric machines neglected the static eccentricity, and the others considered it to study the vibration characteristics, usually paying attention to the dynamic response by numerical method. However, this method cannot offer insight into the vibration influenced by UMP. Furthermore, most of the electrical machines studied in these papers have a narrow speed range. However, the speed of PMSMs in HEVs and EVs varies with external loads in a large range. Due to static eccentricity, the complexity of dynamic behaviors further increases. The excitations deriving from road roughness and the internal combustion engine will impact on the rotor. These external loads with a wide frequency band may lead to the resonance of the rotor system, which decreases the performance of the rotor system. Therefore, the vibration characteristics of the PMSMs caused by static eccentricity and UMP should be scrutinized by an analytical method.

This paper focuses on the asymmetric effect of nonlinear vibration of the rotor system of PMSMs in HEVs and EVs caused by static eccentricity. In Sect. 2, the UMP model is selected, and the Jeffcott rotor model is applied to the rotor system. In Sect. 3, the influences of static eccentricity and UMP on the static characteristics of the rotor system are investigated, and stability analysis is performed. The corresponding bifurcation diagrams are plotted. In Sect. 4, the steady-state analytical solution and frequency characteristics of the main resonance are studied by multi-scale method. The stability of the solution is analyzed by Routh–Hurwitz criterion and the geometric constraint. The influences of the system parameters, such as the stiffness ratio, damping ratio, mass eccentricity ratio and static eccentricity ratio, on the frequency characteristics are analyzed. The results of the multi-scale method are validated by

a numerical method. Conclusions are summarized in Sect. 5.

2 Mathematical model

In this paper, the following assumptions are adopted:

- (a) The rotor is mounted at the midspan of the two bearings supporting the rotor shaft, and the air gap is identical along the axial direction.
- (b) The vibration of the stator is neglected.
- (c) The mass eccentricity and static radial eccentricity of the rotor exist.

2.1 UMP model

In this paper, we adopt the model of UMP in reference [14]. Furthermore, the pole-pair number in the PMSMs of HEVs and EVs is usually more than 3, and the UMP expression is

$$f_u = \frac{RL\pi F_m^2}{4\mu_0} (2\Lambda_0\Lambda_1 + \Lambda_1\Lambda_2 + \Lambda_2\Lambda_3) \quad (1)$$

where μ_0 is the air permeability, R is the rotor core outer radius, L is the rotor core length, Λ_n is the coefficient of the Fourier series of air-gap permeance and F_m is the fundamental MMF amplitude. Λ_n and F_m can be determined by the following formulae:

$$\Lambda_n = \begin{cases} \frac{\mu_0}{\delta_0} \frac{1}{\sqrt{1-\varepsilon^2}} & n = 0 \\ \frac{2\mu_0}{\delta_0} \frac{1}{\sqrt{1-\varepsilon^2}} \left(\frac{1-\sqrt{1-\varepsilon^2}}{\varepsilon} \right)^n & n = 1, 2, \dots \end{cases} \quad (2)$$

where δ_0 is the average air-gap length, the non-dimensional eccentricity $\varepsilon = r/\delta_0$ is also called non-dimensional radial displacement, and r is the eccentricity of the stator and rotor.

$$F_m = \sqrt{F_{rm}^2 + F_{sm}^2 - 2F_{rm}F_{sm} \sin \varphi_0} \quad (3)$$

where F_{rm} is the fundamental MMF amplitude of the rotor, F_{sm} is the fundamental MMF amplitude of the three-phase winding and φ_0 is the inner power factor angle.

2.2 Dynamic model

According to the above assumptions, an arbitrary cross section can reflect the eccentricity of the stator and

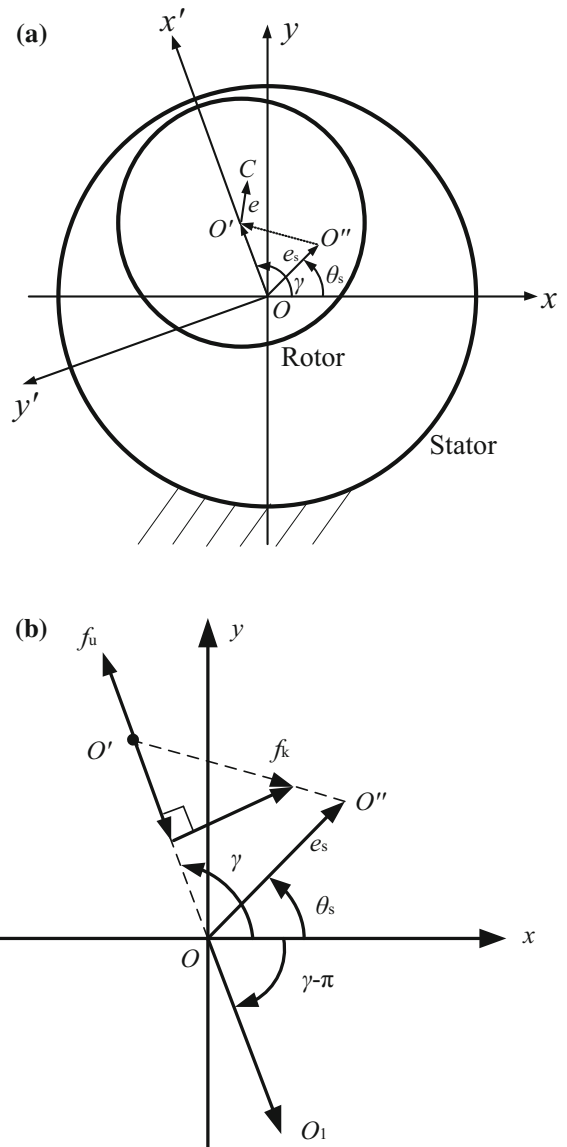


Fig. 1 Scheme of eccentricity between stator and rotor

rotor. For simplicity, we select the cross section at the middle of the span, as shown in Fig. 1a. The stator center O is fixed. Due to assembly error, the centerline of the rotor is not aligned with that of the stator. The rotor centerline deviates from but is parallel with the stator centerline. This deviation is the static radial eccentricity, which can be depicted by the stationary rotor center vector OO'' with amplitude e_s and direction angle θ_s . Due to the mass eccentricity, the rotor center escapes from the point O'' when the rotor spins. Therefore, $Ox'y'$ is a rotating coordinate system that has the same

origin that the inertial coordinate system Oxy . At a general time instant t , the rotor center O' is shown in Fig. 1. The point C is the mass center of the rotor, and $O'C$ is the mass eccentric distance of which the length is denoted by e . The radial eccentricity of the rotor center is OO' , whereas the deformation of the rotor shaft is $O''O'$. Therefore, UMP always acts along the direction from the stator center O to the rotor center O' , while the restoring force of the rotor shaft points to the point O'' from the rotor center O' . The restoring force and UMP are generally not in the same direction.

The vibration system of the rotor is simplified to a Jeffcott rotor, and the corresponding motion equation can be written as:

$$\begin{cases} m\ddot{x} + c\dot{x} + k(x - x_0) - f_u \cos \gamma = m\omega^2 \cos \omega t \\ m\ddot{y} + c\dot{y} + k(y - y_0) - f_u \sin \gamma = m\omega^2 \sin \omega t \end{cases} \quad (4)$$

where m is the rotor mass, c is the damping coefficient, x_0 and y_0 are, respectively, the components of static eccentricity in the x - and y -directions, γ is the direction angle of UMP, ω is the rotor angular speed, and k is the mechanical stiffness of the rotor shaft. According to Fig. 1, $x_0 = e_s \cos \theta_s$, $y_0 = e_s \sin \theta_s$.

Let $\omega_0 = \sqrt{k/m}$ and $\tau = \omega_0 t$. The non-dimensional form of Eq. (4) is

$$\begin{cases} \varepsilon_x'' + 2\xi\varepsilon_x' + \varepsilon_x - \bar{f}_u(\varepsilon) \frac{\varepsilon_x}{\varepsilon} = \beta\bar{\omega}^2 \cos \bar{\omega}\tau + \beta_{sx} \\ \varepsilon_y'' + 2\xi\varepsilon_y' + \varepsilon_y - \bar{f}_u(\varepsilon) \frac{\varepsilon_y}{\varepsilon} = \beta\bar{\omega}^2 \sin \bar{\omega}\tau + \beta_{sy} \end{cases} \quad (5)$$

where $\xi = \frac{c}{2\sqrt{km}}$ is the damping ratio, $\beta = \frac{e}{\delta_0}$ is the mass eccentricity ratio, $\beta_s = \frac{e_s}{\delta_0}$ is the static eccentricity ratio (non-dimensional static eccentricity), $\bar{\omega} = \frac{\omega}{\omega_0}$ is the frequency ratio, $\bar{f}_u(\varepsilon) = \frac{f_u(\varepsilon)}{k\delta_0}$ is the non-dimensional UMP, $\varepsilon_x = x/\delta_0$ and $\varepsilon_y = y/\delta_0$ are the non-dimensional radial displacement components in the x - and y -directions, respectively, $\beta_{sx} = \beta_s \cos \theta_s$ and $\beta_{sy} = \beta_s \sin \theta_s$ are the non-dimensional static eccentricity components in the x - and y -directions, respectively, and $(\cdot)'$ represents the differentiation with respect to the non-dimensional time τ . It can be seen that the first and second terms on the right side in Eq. (5) are the external excitations caused by the mass imbalance and static eccentricity, respectively.

The complex form of Eq. (5) is

$$z'' + 2\xi z' + z - \bar{f}_u(\varepsilon) \frac{z}{|z|} = \beta\bar{\omega}^2 e^{i\bar{\omega}\tau} + z_s \quad (6)$$

where $z = \varepsilon_x + i\varepsilon_y$ is the non-dimensional radial displacement in complex form, $z_s = \beta_s e^{i\theta_s}$ is the non-dimensional static eccentricity in complex form, and i is the imaginary unit.

3 Static characteristics analysis considering static eccentricity

3.1 Characteristics of system conservative force

For the static characteristics of the rotor system, the angular speed is zero, that is, $\bar{\omega} = 0$, yielding

$$z'' + 2\xi z' + z - \bar{f}_u(\varepsilon) \frac{z}{|z|} = z_s \quad (7)$$

As shown in Fig. 1, the non-dimensional form of the radial displacement OO' can be expressed as $z = \varepsilon e^{i\gamma}$. In Fig. 1b, the vector OO_1 with amplitude ε and direction angle $(\gamma - \pi)$ has the non-dimensional form $z = \varepsilon e^{i(\gamma - \pi)}$. For simplicity, OO_1 can be considered as a vector with direction angle γ . Thus, the corresponding amplitude is $-\varepsilon$ of which the sign denotes the opposite direction with respect to OO' . In this section, we specify that the amplitude of the relative radial displacement is permitted to be negative except for a special situation.

According to Eq. (6), for an arbitrary relative radial displacement, the non-dimensional system conservative force is:

$$\bar{f}(z) = z - z_s - \bar{f}_u(\varepsilon) \frac{z}{|z|} \quad (8)$$

It can be seen that $\bar{f}(z)$ is a vector function. Eq. (8) determines a steady planar vector field as shown in Fig. 2. The color and the streamline depict the magnitude and the direction of the force, respectively. For

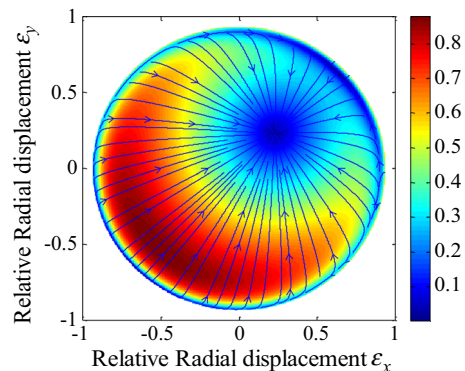


Fig. 2 Vector field of system conservative force

an arbitrary point in this vector field, the corresponding conservative force acts along the tangential direction of the streamline across the point. For simplicity, we decompose the conservative force into two components in the radial and tangential directions of the stator. The two non-dimensional components denoted by $\bar{f}_r(\varepsilon)$ and $\bar{f}_t(\varepsilon)$, respectively, are

$$\begin{cases} \bar{f}_r(\varepsilon) = \varepsilon - \bar{f}_u(\varepsilon) - \beta_s \cos \theta_{di} = \varepsilon - \bar{f}_u(\varepsilon) - \varepsilon_r \\ \bar{f}_t(\varepsilon) = \beta_s \sin \theta_{di} = \varepsilon_t \end{cases} \quad (9)$$

where $\theta_{di} = \gamma - \theta_s$ is the angle from the direction of the static eccentricity (OO'') to that of UMP (OO'), and $\varepsilon_r = \beta_s \cos \theta_{di}$ and $\varepsilon_t = \beta_s \sin \theta_{di}$ are the non-dimensional additional forces in the radial and tangential directions of the stator caused by the static eccentricity, respectively. In addition to the static eccentricity, the two additional forces also depend on the angle θ_{di} , which varies in the range of $[-\pi, \pi]$ according to Fig. 1.

The radial stiffness and the tangential stiffness denoted by $\bar{k}_r(\varepsilon)$ and $\bar{k}_t(\varepsilon)$, respectively, are

$$\begin{cases} \bar{k}_r(\varepsilon) = \bar{k} - \bar{k}_u(\varepsilon) = 1 - \bar{k}_u(\varepsilon) \\ \bar{k}_t(\varepsilon) = 0 \end{cases} \quad (10)$$

where $\bar{k} = 1$ is the non-dimensional mechanical stiffness and $\bar{k}_u(\varepsilon)$ is the non-dimensional electromagnetic stiffness of UMP.

$$\bar{k}_u(\varepsilon) = \frac{df_u(\varepsilon)}{d\varepsilon} = \frac{k_u(\varepsilon)}{k} \quad (11)$$

where $k_u(\varepsilon) = \frac{df_u(\varepsilon)}{dr}$ is the dimensional electromagnetic stiffness. At $\varepsilon = 0$, $\bar{k}_u(\varepsilon)$ attains the minimum value, and thus, $\bar{k}_r(\varepsilon)$ attains the maximum value. Let $\varepsilon = 0$ which then yields

$$\begin{cases} \alpha = \bar{k}_u(0) = \frac{k_u(0)}{k} \\ \bar{k}_{r0} = \bar{k}_r(0) = 1 - \alpha \end{cases} \quad (12)$$

where, $k_u(0) = \left(\frac{df_u(\varepsilon)}{dr}\right)_{r=0} = \frac{1}{2} \frac{\mu_0 RL \pi F_m^2}{\delta_0^3}$. The parameter α that represents the non-dimensional electromagnetic stiffness at $\varepsilon = 0$ can be called the stiffness ratio according to the first formula in Eq. (12). Physically, the parameter α is the ratio of the electromagnetic stiffness at $\varepsilon = 0$ to the mechanical stiffness, which gives a comparison of the two stiffnesses. $\alpha = 1$ is a critical value that represents that the electromagnetic stiffness at $\varepsilon = 0$ is equal to the mechanical stiffness. $\alpha < 1$ represents that the electromagnetic stiffness at

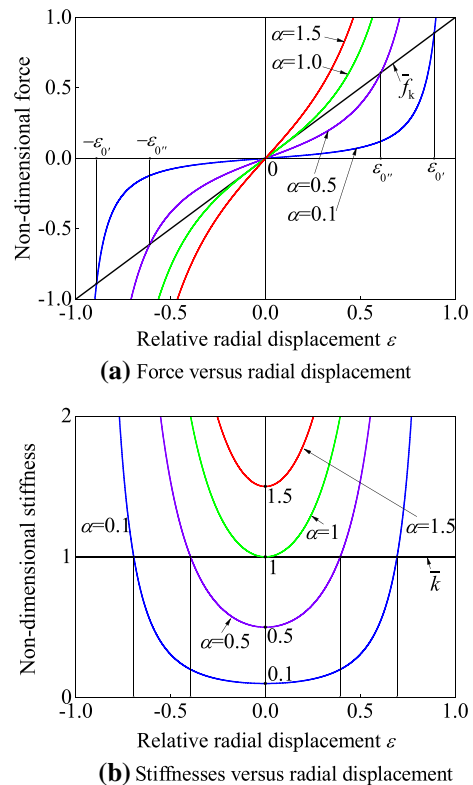


Fig. 3 Force and stiffness characteristics

$\varepsilon = 0$ is less than the mechanical stiffness, and vice versa for $\alpha > 1$. According to the Taylor formula, we expand $\bar{f}_u(\varepsilon)$ as a polynomial at $\varepsilon = 0$, and keep the first three order terms, yielding

$$\bar{f}_u(\varepsilon) \approx \alpha \varepsilon + \frac{3\alpha}{2} \varepsilon^3 \quad (13)$$

From Eq. (1), UMP is an odd function, and thus, the corresponding electromagnetic stiffness is an even function. UMP and its stiffness varying with α are shown in Fig. 3. Furthermore, UMP and its electromagnetic stiffness provide larger slopes as the magnitude of the radial displacement increases.

It can be seen that the system stiffness is independent of the static eccentricity that plays a significant role in the conservative force from Eqs. (9) and (10). The radial force $\bar{f}_r(\varepsilon)$ influenced by the static eccentricity varies with the radial displacement as shown in Fig. 4. This discussion will be performed in the range of the angle from OO'' (static eccentricity) to the line OO' , i.e., $\theta_{di} \in [0, \pi]$ due to the symmetry of the additional radial force ε_r with respect to the static eccentricity OO'' according to Fig. 1 and Eq. (9). When the angle

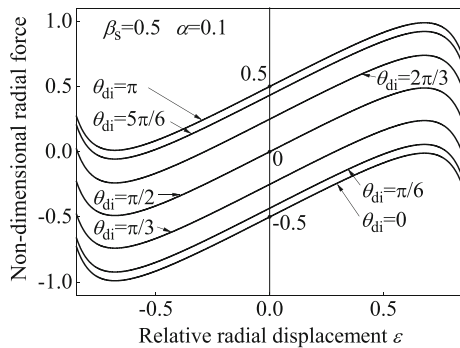


Fig. 4 Radial component of system conservative force

θ_{di} is 0, the tangential force \bar{f}_t that is the additional tangential force ε_t vanishes, and therefore, the system conservative force is identical to the radial force \bar{f}_r , and the additional radial force ε_r reaches the maximum value. Thus, the rotor center O' is located in the line OO'' , and the action line of UMP coincides with that of the restoring force. However, when θ_{di} is $\pi/2$, the additional tangential force ε_t reaches the maximum value, and the additional radial force ε_r is 0.

According to the above analysis, the equilibrium point of the system should be in the line OO'' , i.e., $\gamma = \theta_s$. For the simplicity of the analysis of the equilibrium point, we only discuss the conservative force along the direction of the line OO'' . In this direction, the system conservative force is

$$\bar{f}(\varepsilon) = \varepsilon - \beta_s - \bar{f}_u(\varepsilon) = \bar{f}_k(\varepsilon) - \bar{f}_u(\varepsilon) \tag{14}$$

where $\bar{f}_k(\varepsilon) = \varepsilon - \beta_s$ is the non-dimensional restoring force along the direction of the line OO'' .

According to Eqs. (13) and (14), UMP depends on the stiffness ratio α , and the restoring force depends on the static eccentricity ratio β_s . However, their stiffnesses are independent of β_s . In light of Eqs. (10), (12) and the above analysis, for the case of $\alpha > 1$, the system stiffness, of which zero points do not exist, is always negative, and thus, the system undergoes the loss of stability. The system conservative force $\bar{f}(\varepsilon)$ has only one unstable zero point denoted by ε_s . $\alpha < 1$ ensures that the rotor system has a positive stiffness interval $(-\varepsilon_1, \varepsilon_1)$, of which the two endpoints are the zero points of the system stiffness and hence the extreme points of the force that are independent of the static eccentricity ratio β_s , as shown in Fig. 5a. The smaller the stiffness ratio α is, the wider the interval. Assuming that $\beta_s = 0$ (without static eccentricity), the system conservative force $\bar{f}(\varepsilon)$ has three zero points denoted by $\varepsilon_s, \varepsilon_{u1}$ and

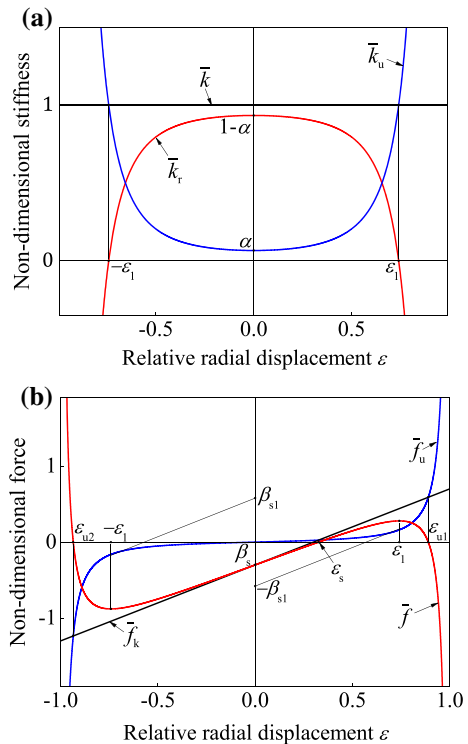


Fig. 5 UMP, restoring force and system conservative force and their stiffnesses versus radial displacement. **a** Stiffness versus radial displacement ($\alpha < 1$): the line $\bar{k} = 1$ denotes the non-dimensional stiffness of the rotor shaft (mechanical stiffness); the curve \bar{k}_u (blue curve) that passes through the point $(0, \alpha)$ represents the non-dimensional UMP stiffness (electromagnetic stiffness); and the curve \bar{k}_r (red curve) that passes through the points $(0, 1 - \alpha)$, $(-\varepsilon_1, 0)$ and $(\varepsilon_1, 0)$ denotes the non-dimensional system stiffness, where $\pm\varepsilon_1$ are the zero points of the non-dimensional system stiffness. **b** Force versus radial displacement ($\alpha < 1, -\beta_{s1} < \beta_s < \beta_{s1}$): the line \bar{f}_k , the curve \bar{f}_u (blue curve) and the curve \bar{f} (red curve) denote the non-dimensional restoring force, UMP and system conservative force, respectively. $\varepsilon_s, \varepsilon_{u1}$ and ε_{u2} are the zero points of the non-dimensional system conservative force. β_{s1} is the critical static eccentricity ratio. The lines that pass through the points $(0, \beta_{s1})$ or $(0, -\beta_{s1})$ are tangential to the curve \bar{f}_u and parallel to the line \bar{f}_k . $\pm\varepsilon_1$ are the extreme points of the non-dimensional system conservative force.

ε_{u2} . Furthermore, $\varepsilon_s = 0$ and $\varepsilon_{u1} = -\varepsilon_{u2}$ because $\bar{f}(\varepsilon)$ is an odd function for the case of $\beta_s = 0$. Therefore, for fixed $\beta_s = 0$, $\alpha = 1$ is a critical value. When the stiffness ratio α increases and passes through 1, the number of zero points of $\bar{f}(\varepsilon)$ increases from 1 to 3. As shown in Fig. 5b, for $\alpha < 1$, when the static eccentricity ratio β_s increases from 0, the restoring force $\bar{f}_k(\varepsilon) = \varepsilon - \beta_s$ moves down and the zero points ε_{u1} and ε_{u2} are no longer symmetric with respect to ε_s . Moreover, $\varepsilon_s \neq 0$. The former two points are unstable, whereas the latter one is

stable. As β_s increases to β_{s1} , the restoring force $\bar{f}_k(\varepsilon)$ is tangential to the UMP curve so that $\bar{f}(\varepsilon_1) = 0$, and the zero points ε_s and ε_{u1} , which coincide with the system stiffness zero point ε_1 together with ε_{u2} , are unstable. The number of zero points decreases to 2, i.e., ε_1 and ε_{u2} . Therefore, the parameter β_{s1} is critical to this number. With the increase in β_s , $\beta_s > \beta_{s1}$ holds, and the zero point ε_1 disappears. The other zero point ε_{u2} is still unstable. For $\beta_s < 0$, when $\beta_s = -\beta_{s1}$, ε_s and ε_{u2} coincide with each other, and both are equal to $-\varepsilon_1$. At this time, both $-\varepsilon_1$ and ε_{u1} are unstable. The former zero point disappears for $\beta_s < -\beta_{s1}$. According to this analysis, we can yield

$$\pm \beta_{s1} = \pm[\varepsilon_1 - \bar{f}_u(\varepsilon_1)] \tag{15}$$

This parameter β_{s1} can be called the critical static eccentricity ratio, and the critical dimensional static eccentricities are

$$\pm e_{s1} = \pm\beta_{s1}\delta_0 = \pm[kr_1 - f_u(\varepsilon_1)]/k \tag{16}$$

where, $r_1 = \varepsilon_1\delta_0$. According to Eq. (16), e_{s1} is equal to the equivalent deformation produced by the extremum of the system conservative force without static eccentricity applying to the rotor shaft. Therefore, the analysis provides two stability conditions for a practical system: $\alpha < 1$ and $|\beta_s| < \beta_{s1}$, as shown in Fig. 5b. The former is a stiffness condition that ensures that the rotor system has a positive stiffness interval $(-\varepsilon_1, \varepsilon_1)$, of which the endpoints are independent of β_s . Outside the interval $[-\varepsilon_1, \varepsilon_1]$, the system stiffness is negative which leads to the contact of rotor and stator easily. The latter is an eccentricity condition. Under the prerequisite of the first condition, the latter ensures that the rotor system has at least one stable zero point (equilibrium point).

3.2 Stability analysis and bifurcation

The zero points of the conservative force correspond to the system equilibrium points. We can use Lyapunov method to determine their stabilities easily for the common equilibrium points. However, according to the analysis in Sect. 3.1, the equilibrium points $\varepsilon_s = 0$ ($\beta_s = 0, \alpha = 1$), $\varepsilon_s = \varepsilon_{u1} = \varepsilon_1$ ($\beta_s = \beta_{s1}, \alpha < 1$) and $\varepsilon_s = \varepsilon_{u2} = -\varepsilon_1$ ($\beta_s = -\beta_{s1}, \alpha < 1$) are the critical cases, and the corresponding Jacobi matrices all have zero eigenvalues, and the other eigenvalues all have negative real parts. The stabilities of these equilibrium points cannot be determined according to

this method. Therefore, the center manifold theorem should be adopted. The analysis process for $\varepsilon_s = \varepsilon_{u1} = \varepsilon_1$ ($\beta_s = \beta_{s1}, \alpha < 1$) is given below.

For the case of $\varepsilon_s = \varepsilon_{u1} = \varepsilon_1$ ($\beta_s = \beta_{s1}, \alpha < 1$), the two equilibrium points coincide with the extreme point of the conservative force ε_1 . To simplify the calculation, we assume that the rotor center only whirls along the direction of the static eccentricity (OO''). Therefore, Eq. (7) degrades into

$$\varepsilon'' + 2\xi\varepsilon' + \varepsilon - \beta_{s1} - \bar{f}_u(\varepsilon) = 0 \tag{17}$$

To perform center manifold theorem, we select the equilibrium point as a new origin and then apply the translation transformation to Eq. (17). Thus, the corresponding state equation is

$$\mathbf{y}' = \mathbf{G}(\mathbf{y}) \tag{18}$$

where $\mathbf{y} = \begin{bmatrix} y_1 \\ y_2 \end{bmatrix}$, $\mathbf{y}' = \begin{bmatrix} y_1' \\ y_2' \end{bmatrix}$, and $\mathbf{G}(\mathbf{y}) = \begin{bmatrix} y_2 \\ -2\xi y_2 - (y_1 + \varepsilon_1) + \bar{f}_u(y_1 + \varepsilon_1) + \beta_{s1} \end{bmatrix}$.

The Taylor expansion of $\bar{f}_u(y_1 + \varepsilon_1)$ is

$$\bar{f}_u(y_1 + \varepsilon_1) = \varepsilon_1 - \beta_{s1} + y_1 + \delta_2 y_1^2 + \delta_3 y_1^3 + \delta_4 y_1^4 + \dots \tag{19}$$

where, $\delta_i = \left. \frac{d^i \bar{f}_u(\varepsilon)}{2d\varepsilon^{(i)}} \right|_{\varepsilon=\varepsilon_1} = \left. \frac{d^i \bar{f}_u^{(i)}(y_1+\varepsilon_1)}{2d\varepsilon^{(i)}} \right|_{y_1=0}$. Clearly, $\delta_2 > 0$ holds due to the stiffness of UMP being a convex function (Fig. 5b). The system determined by Eq. (18) has only one equilibrium point at $y_1 = y_2 = 0$. The Jacobi matrix at this equilibrium point is

$$\mathbf{J} = \begin{bmatrix} 0 & 1 \\ 0 & -2\xi \end{bmatrix}.$$

The eigenvalues and eigenvectors of the matrix are, respectively,

$$\lambda_1 = 0, \mathbf{p}_1 = [1, 0]^T; \lambda_2 = -2\xi, \mathbf{p}_2 = [1, \lambda_2]^T.$$

We define a transformation as

$$[y_1, y_2]^T = [\mathbf{p}_1, \mathbf{p}_2][u, v]^T = [u + v, -2\xi v]^T \tag{20}$$

Substituting Eq. (20) into Eq. (18) yields

$$\begin{cases} u' = -\frac{1}{2\xi}[(u + v + \varepsilon_1 - \beta_{s1}) - \bar{f}_u(u + v + \varepsilon_1)] \\ v' = -2\xi v + \frac{1}{2\xi}[(u + v + \varepsilon_1 - \beta_{s1}) - \bar{f}_u(u + v + \varepsilon_1)] \end{cases} \tag{21}$$

Substituting Eq. (19) into Eq. (21), and combining Eq. (20), yields

$$\begin{cases} u' = g(u, v) \\ v' = -2\xi v - g(u, v) \end{cases} \tag{22}$$

where, $g(u, v) = \frac{1}{2\xi}[\delta_2(u+v)^2 + \delta_3(u+v)^3 + \delta_4(u+v)^4 + \dots]$ is a nonlinear function excluding the linear term. According to Eq. (22), we can obtain

$$g(0, 0) = 0, \quad \left. \frac{\partial g}{\partial u} \right|_{u=0, v=0} = 0, \quad \left. \frac{\partial g}{\partial v} \right|_{u=0, v=0} = 0 \tag{23}$$

According to the center manifold theorem, there exists a center manifold for Eq. (21), which can be expressed as the function $v = h(u)$, which then yields

$$h(0) = 0, \quad \left. \frac{\partial h}{\partial u} \right|_{u=0} = 0 \tag{24}$$

Substituting this function into Eq. (21), the equation of the center manifold is carried out as below.

$$\left(\frac{dh}{du} + 1 \right) u' + 2\xi h = 0 \tag{25}$$

Assume that the Taylor expansion of h has the following form:

$$h = au^2 \tag{26}$$

Substituting Eq. (26) into Eq. (25) and using Eqs. (19) and (21) yields

$$a = -\frac{\delta_2}{4\xi^2} \tag{27}$$

Thus, we can obtain the reduced system

$$u' = \frac{\delta_2}{2\xi} \left(u - \frac{\delta_2}{4\xi^2} u^2 \right)^2 \tag{28}$$

Due to $\delta_2 > 0$, the equilibrium point $u = 0$ of the reduced system in Eq. (28), is unstable. Therefore, the equilibrium point of the original system in Eq. (18) is unstable, and hence, the equilibrium point $\varepsilon_s = \varepsilon_{u1} = \varepsilon_1$ according to center manifold theorem. For the equilibrium points $\varepsilon_s = \varepsilon_{u2} = -\varepsilon_1$ ($\beta_s = -\beta_{s1}, \alpha < 1$) and $\varepsilon_s = 0$ ($\beta_s = 0, \alpha = 1$), a similar procedure can also be performed by this method, and the results show that both equilibrium points are unstable. As the parameters α and β_s cross these critical values, the static bifurcation occurs as shown in Fig. 6. When the static eccentricity ratio $\beta_s = 0$ remains unchanged and the stiffness ratio α passes through 1, a pitchfork bifurcation occurs as shown in Fig. 6a. When the static eccentricity increases from 0, the pitchfork bifurcation is destroyed, and then a generic bifurcation with a defect occurs. Therefore, β_s is an unfolding parameter. For a comparatively large β_s , the curve becomes single-valued. Therefore, a pair of saddle-node bifurcations occurs as β_s varies (Fig. 6b).

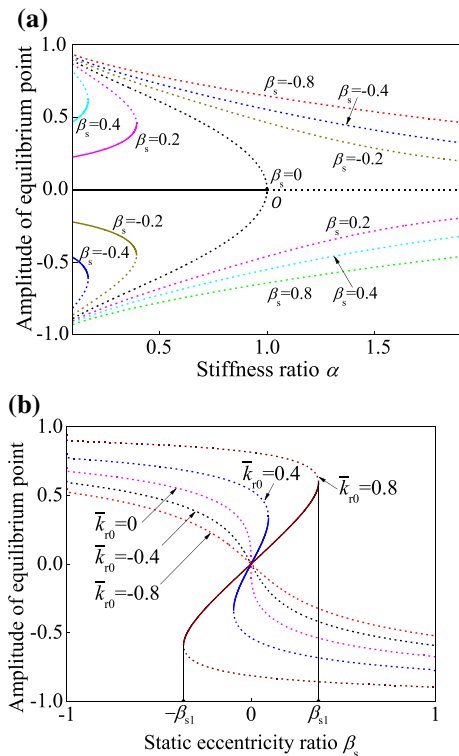


Fig. 6 Bifurcation diagrams

4 Forced response influenced by static eccentricity

The static eccentricity spoils the symmetry of the system conservative force and hence the equilibrium point. Moreover, this asymmetry has a dynamic effect on the rotor system. In this section, we will discuss this effect. For the simplicity of the analysis, substituting Eq. (13) into Eq. (6) yields

$$z'' + 2\xi z' + \omega_g^2 z - \varepsilon_P z^2 \bar{z} = \beta \bar{\omega}^2 e^{i\bar{\omega}\tau} + z_s \tag{29}$$

where $\omega_g = \sqrt{1 - \alpha}$ is the natural frequency of the generating system of Eq. (6), and $\varepsilon_P = \frac{3\alpha}{2}$ is the nonlinear parameter. According to the static analysis in Sect. 3, the stiffness ratio α is a small parameter and hence ε_P for a practical system with adequate stability margin.

4.1 Vibration characteristics without static eccentricity

Considering the mass imbalance and neglecting the static eccentricity, the frequency characteristics can be obtained by using harmonic balance method.

$$\begin{cases} (\varepsilon^2 - \beta^2)\bar{\omega}^4 + \left[4\xi^2 - 2\left(1 - \alpha - \frac{3\alpha\varepsilon^2}{2}\right)\right]\varepsilon^2\bar{\omega}^2 \\ + \left(1 - \alpha - \frac{3\alpha\varepsilon^2}{2}\right)^2\varepsilon^2 = 0 \\ \tan \varphi = \frac{-2\xi\bar{\omega}}{1 - \alpha - \frac{3\alpha\varepsilon^2}{2} - \bar{\omega}^2} \end{cases} \quad (30)$$

According to the analysis of harmonic balance method, only the fundamental harmonic component exists in the system response. Therefore, the steady-state periodic solution of Eq. (29) is

$$z = \varepsilon e^{i(\bar{\omega}\tau + \varphi)} \quad (31)$$

Substituting Eq. (31) into Eq. (29) and using averaging method, yields

$$\begin{cases} \varepsilon' = -2\xi\varepsilon - \beta\bar{\omega} \sin \varphi \\ \varphi' = \frac{1 - \alpha - \frac{3\alpha\varepsilon^2}{2}}{\bar{\omega}} - \frac{\beta\bar{\omega} \cos \varphi}{\varepsilon} - \bar{\omega} \end{cases} \quad (32)$$

For the steady state, we assume that both the amplitude and phase are time-invariant, i.e., $\varepsilon' = 0$ and $\varphi' = 0$. Substituting these two equations into Eqs. (32), (30) is obtained again, which denotes that this assumption is reasonable.

4.2 Vibration characteristics considering static eccentricity

In this section, we discuss the main resonance influenced by static eccentricity. For a system without static eccentricity, we can conveniently use harmonic balance method due to the symmetry of the system. However, for a system with static eccentricity, it is difficult to apply this method to such an asymmetric system. Here, multi-scale method is employed to determine a first-order approximation to the solution of Eq. (29) in the form

$$z = z_0(T_0, T_1) + \varepsilon_P z_1(T_0, T_1) \quad (33)$$

where, $T_0 = \tau, T_1 = \varepsilon_P \tau$. It follows that the derivatives of a function have the following forms:

$$\begin{cases} \frac{d}{d\tau} = D_0 + \varepsilon_P D_1 \\ \frac{d^2}{d\tau^2} = D_0^2 + 2\varepsilon_P D_0 D_1 \end{cases} \quad (34)$$

where $D_0 = \frac{\partial}{\partial T_0}$ and $D_1 = \frac{\partial}{\partial T_1}$.

4.2.1 Analytical solution

Considering that both the damping ratio ξ and the amplitude of the dynamic excitation $\beta\bar{\omega}^2 e^{i\bar{\omega}\tau}$ are small and have an accuracy of $O(\varepsilon_P)$, let

$$\begin{cases} \xi = \xi_1 \varepsilon_P \\ \beta = \beta_1 \varepsilon_P \end{cases} \quad (35)$$

To investigate the main resonance, we introduce the detuning parameter σ_1 , which quantitatively describes the nearness of the excitation frequency $\bar{\omega}$ to the natural frequency of the generating system ω_g . Accordingly, we can write

$$\bar{\omega}^2 = \omega_g^2 + \sigma_1 \varepsilon_P \quad (36)$$

Substituting Eqs. (36) and (33) into Eq. (29) and then using Eq. (36) to eliminate the parameter ω_g yields order ε_P^0 :

$$D_0^2 z_0 + \bar{\omega}^2 z_0 = z_s \quad (37)$$

and order ε_P^1 :

$$D_0^2 z_1 + \bar{\omega}^2 z_1 = -2D_0 D_1 z_0 - 2\xi_1 D_0 z_0 + \beta_1 \bar{\omega}^2 e^{i\bar{\omega}T_0} + \sigma_1 z_0 + z_0^2 \bar{z}_0 \quad (38)$$

We can determine the free vibration solution of Eq. (37) in the form

$$z_{0F} = A_1(T_1)e^{i\bar{\omega}T_0} + A_2(T_1)e^{-i\bar{\omega}T_0} \quad (39)$$

where, $A_1(T_1)$ and $A_2(T_1)$ are the complex amplitudes of the forward and backward whirling motions, respectively. Both are functions with respect to the time scale T_1 .

The forced response of the system of Eq. (37) caused by the static eccentricity is

$$z_{0S} = \frac{z_s}{\bar{\omega}^2} = \frac{\beta_s e^{i\theta_s}}{\bar{\omega}^2} \quad (40)$$

Therefore, the general solution of Eq. (37) is written as:

$$z_0 = z_{0F} + z_{0S} \quad (41)$$

Substituting z_0 into Eq. (38), then yields

$$D_0^2 z_1 + \bar{\omega}^2 z_1 = E_{\bar{\omega}} e^{i\bar{\omega}T_0} + E_{-\bar{\omega}} e^{-i\bar{\omega}T_0} + E_{2\bar{\omega}} e^{2i\bar{\omega}T_0} + E_{-2\bar{\omega}} e^{-2i\bar{\omega}T_0} + E_{3\bar{\omega}} e^{3i\bar{\omega}T_0} + E_{-3\bar{\omega}} e^{-3i\bar{\omega}T_0} + E_S \quad (42)$$

where,

$$\begin{aligned}
 E_{\bar{\omega}} &= -2i\bar{\omega}(D_1 A_1 + \xi_1 A_1) + A_1|A_1|^2 \\
 &\quad + 2A_1|A_2|^2 + 2A_1|z_{0S}|^2 + \bar{A}_2 z_{0S}^2 \\
 &\quad + \sigma_1 A_1 + \beta_1 \bar{\omega}^2, \\
 E_{-\bar{\omega}} &= 2i\bar{\omega}(D_1 A_2 + \xi_1 A_2) + A_2|A_2|^2 \\
 &\quad + 2A_2|A_1|^2 + 2A_2|z_{0S}|^2 + \bar{A}_1 z_{0S}^2 + \sigma_1 A_2, \\
 E_{2\bar{\omega}} &= A_1^2 \bar{z}_{0S} + 2A_1 \bar{A}_2 z_{0S}, \\
 E_{-2\bar{\omega}} &= A_2^2 \bar{z}_{0S} + 2\bar{A}_1 A_2 z_{0S}, \quad E_{3\bar{\omega}} = A_1^2 \bar{A}_2, \\
 E_{-3\bar{\omega}} &= \bar{A}_1 A_2^2,
 \end{aligned}$$

and

$$\begin{aligned}
 E_S &= \sigma_1 z_{0S} + 2z_{0S}(|A_1|^2 + |A_2|^2) \\
 &\quad + 2A_1 A_2 \bar{z}_{0S} + |z_{0S}|^2 z_{0S}.
 \end{aligned}$$

Both $E_{\bar{\omega}}e^{i\bar{\omega}T_0}$ and $E_{-\bar{\omega}}e^{-i\bar{\omega}T_0}$ are secular terms that should be avoided. Let

$$\begin{cases} E_{\bar{\omega}} = 0 \\ E_{-\bar{\omega}} = 0 \end{cases} \tag{43}$$

After eliminating the secular terms, the right side of Eq. (42) has five residual terms, $E_{2\bar{\omega}}e^{2i\bar{\omega}T_0}$, $E_{-2\bar{\omega}}e^{-2i\bar{\omega}T_0}$, $E_{3\bar{\omega}}e^{3i\bar{\omega}T_0}$, $E_{-3\bar{\omega}}e^{-3i\bar{\omega}T_0}$ and E_S . The responses of Eq. (42) caused by these terms are listed as follows:

$$\begin{cases} z_{2\bar{\omega}} = -\frac{E_{2\bar{\omega}}}{3\bar{\omega}^2} e^{2i\bar{\omega}T_0} \\ z_{-2\bar{\omega}} = -\frac{E_{-2\bar{\omega}}}{3\bar{\omega}^2} e^{-2i\bar{\omega}T_0} \\ z_{3\bar{\omega}} = -\frac{E_{3\bar{\omega}}}{8\bar{\omega}^2} e^{3i\bar{\omega}T_0} \\ z_{-3\bar{\omega}} = -\frac{E_{-3\bar{\omega}}}{8\bar{\omega}^2} e^{-3i\bar{\omega}T_0} \\ z_{ES} = \frac{E_S}{\bar{\omega}^2} \end{cases} \tag{44}$$

The solution of the first-order approximate equation in Eq. (42) is

$$z_1 = z_{2\bar{\omega}} + z_{-2\bar{\omega}} + z_{3\bar{\omega}} + z_{-3\bar{\omega}} + z_{ES} \tag{45}$$

According to Eqs. (33), (41) and (45), the solution of the rotor system can be written as:

$$\begin{aligned}
 z &= z_{0F} + z_{0S} \\
 &\quad + \varepsilon_P(z_{2\bar{\omega}} + z_{-2\bar{\omega}} + z_{3\bar{\omega}} + z_{-3\bar{\omega}} + z_{ES}) \tag{46}
 \end{aligned}$$

Compared with the case without static eccentricity, this response includes not only the higher harmonic components but also the backward whirling motion in addition to the forward whirling motion. From Eqs. (42), (44) and (46), we can observe the coupling of the forward and backward whirling motions.

4.2.2 Frequency characteristics of the main resonance

According to Eq. (43), we can obtain

$$\begin{cases} D_1 A_1 = -\xi_1 A_1 - \frac{i}{2\bar{\omega}} \\ \quad [A_1|A_1|^2 + 2A_1|A_2|^2 + 2A_1|z_{0S}|^2 \\ \quad \quad + \bar{A}_2 z_{0S}^2 + \sigma_1 A_1 + \beta_1 \bar{\omega}^2] \\ D_1 A_2 = -\xi_1 A_2 + \frac{i}{2\bar{\omega}} \\ \quad [A_2|A_2|^2 + 2A_2|A_1|^2 + 2A_2|z_{0S}|^2 \\ \quad \quad + \bar{A}_1 z_{0S}^2 + \sigma_1 A_2] \end{cases} \tag{47}$$

According to Eqs. (34) and (39), the derivatives of A_1 and A_2 with respect to τ are listed as follows:

$$\begin{cases} \frac{dA_1}{d\tau} = \varepsilon_P D_1 A_1 \\ \frac{dA_2}{d\tau} = \varepsilon_P D_1 A_2 \end{cases} \tag{48}$$

Let $A_1 = r_1 e^{i\theta_1}$, $A_2 = r_2 e^{i\theta_2}$, and $z_{0S} = r_0 e^{i\theta_s}$, where $r_0 = \frac{\beta_s}{\bar{\omega}^2}$. Substituting these expressions and Eq. (47) into Eq. (48) and then separating the real and imaginary parts yield

$$\begin{cases} r_1' = \varepsilon_P \left[-\xi_1 r_1 + \frac{r_0^2 r_2}{2\bar{\omega}} \sin(2\theta_0 - \theta_1 - \theta_2) \right. \\ \quad \left. - \frac{\bar{\omega} \beta_1}{2} \sin \theta_1 \right] \\ r_1 \theta_1' = -\frac{\varepsilon_P}{2\bar{\omega}} [r_1^3 + 2r_1 r_2^2 + 2r_0^2 r_1 \\ \quad + r_0^2 r_2 \cos(2\theta_0 - \theta_1 - \theta_2) \\ \quad + \bar{\omega}^2 \beta_1 \cos \theta_1 + \sigma_1 r_1] \\ r_2' = \varepsilon_P \left[-\xi_1 r_2 - \frac{r_0^2 r_1}{2\bar{\omega}} \sin(2\theta_0 - \theta_1 - \theta_2) \right] \\ r_2 \theta_2' = \frac{\varepsilon_P}{2\bar{\omega}} [r_2^3 + 2r_1^2 r_2 + 2r_0^2 r_2 \\ \quad + r_0^2 r_1 \cos(2\theta_0 - \theta_1 - \theta_2) + \sigma_1 r_2] \end{cases} \tag{49}$$

From Eq. (49), it can be seen that the amplitudes and phases are dependent on each other. For the steady state, we only assume that $r_1' = 0$ and $r_2' = 0$. From the third formula in Eq. (49), the phase $(2\theta_0 - \theta_1 - \theta_2)$ should be time-invariant and hence phase θ_1 according to the first formula in this equation yields

$$\theta_1' = \theta_2' = 0 \tag{50}$$

Unlike the case without static eccentricity, Eq. (50) is derived by analysis rather than assumption, although the phases are still time-invariant. Usually, in a single degree of freedom system, we assume that both the derivatives of the amplitude and phase with respect to time are equal to 0 for the steady state. This assumption can be further applied to the case without static eccentricity in which there only exists the forward whirling motion. However, for the case considering the static eccentricity, the backward whirling motion appears, and we only assume that the amplitudes of the two whirling motions are time-invariant, whereas the variations of the phases are carried out based on this assumption. As a result, Eq. (50) together with this assumption is validated in Sect. 4.2.4.

Substituting Eq. (50) into Eq. (49), we can get

$$\begin{cases} -\xi_1 r_1 + \frac{r_0^2 r_2}{2\bar{\omega}} \sin(2\theta_0 - \theta_1 - \theta_2) \\ \quad - \frac{\bar{\omega}\beta_1}{2} \sin\theta_1 = 0 \\ r_1^3 + 2r_1 r_2^2 + 2r_0^2 r_1 + r_0^2 r_2 \cos(2\theta_0 - \theta_1 - \theta_2) \\ \quad + \bar{\omega}^2 \beta_1 \cos\theta_1 + \sigma_1 r_1 = 0 \\ \xi_1 r_2 + \frac{r_0^2 r_1}{2\bar{\omega}} \sin(2\theta_0 - \theta_1 - \theta_2) = 0 \\ r_2^3 + 2r_1^2 r_2 + 2r_0^2 r_2 + r_0^2 r_1 \cos(2\theta_0 - \theta_1 - \theta_2) \\ \quad + \sigma_1 r_2 = 0 \end{cases} \quad (51)$$

Eliminating the trigonometric functions in Eq. (51), the frequency characteristics are obtained:

$$\begin{cases} \left[(r_1^2 - r_2^2)^2 - \beta^2 r_1^2 \right] \bar{\omega}^4 \\ \quad + \left[4\xi^2 (r_1^2 + r_2^2)^2 + 2a_m (r_1^2 - r_2^2)^2 \right] \bar{\omega}^2 \\ \quad + a_m^2 (r_1^2 - r_2^2)^2 = 0 \\ r_2^2 \bar{\omega}^4 + r_2^2 (4\xi^2 + 2b_m) \bar{\omega}^2 + r_2^2 b_m^2 - r_0^4 r_1^2 \varepsilon_p^2 = 0 \end{cases} \quad (52)$$

where, $a_m = \varepsilon_P(r_1^2 + r_2^2 + 2r_0^2) - \omega_g^2$ and $b_m = \varepsilon_P(2r_1^2 + r_2^2 + 2r_0^2) - \omega_g^2$ are the parameters defined for simplicity. We can use Routh–Hurwitz criterion to determine the stability of the solution. The Jacobi matrix corresponding to Eq. (49) is written as

$$J_M = [a_{ij}] \quad i = 1, 2, 3, 4, \quad j = 1, 2, 3, 4$$

where,

$$\begin{aligned} a_{11} &= a_{22} = a_{33} = a_{44} = a_{42} = -\xi, \\ a_{12} &= \frac{\varepsilon_P r_1 (2r_0^2 + r_1^2 + 2r_2^2 + \sigma_1)}{2\bar{\omega}}, \quad a_{13} = -\frac{\xi r_2}{r_1}, \\ a_{14} &= \frac{\varepsilon_P r_2^2 (2r_0^2 + 2r_1^2 + r_2^2 + \sigma_1)}{2\bar{\omega} r_1}, \\ a_{21} &= -\frac{\varepsilon_P (2r_0^2 + 3r_1^2 + 2r_2^2 + \sigma_1)}{2\bar{\omega} r_1}, \\ a_{23} &= \frac{\varepsilon_P r_2 (2r_0^2 - 2r_1^2 + r_2^2 + \sigma_1)}{2\bar{\omega} r_1^2}, \\ a_{24} &= \xi \left(\frac{r_2}{r_1} \right)^2, \quad a_{31} = -a_{13}, \\ a_{32} &= -\frac{\varepsilon_P r_2 (2r_0^2 + 2r_1^2 + r_2^2 + \sigma_1)}{2\bar{\omega}}, \\ a_{34} &= a_{32}, \quad a_{41} = -\frac{\varepsilon_P (2r_0^2 - 2r_1^2 + r_2^2 + \sigma_1)}{2\bar{\omega} r_1}, \end{aligned}$$

and

$$a_{43} = \frac{\varepsilon_P (2r_0^2 + 2r_1^2 + 3r_2^2 + \sigma_1)}{2\bar{\omega} r_2}.$$

The characteristic equation is

$$a_0 \lambda^4 + a_1 \lambda^3 + a_2 \lambda^2 + a_3 \lambda + a_4 = 0 \quad (53)$$

where $a_k = (-1)^k tr^{[k]}(J_M)$ and $tr^{[k]}(J_M)$ is k th-order trace of matrix J_M .

$$tr^{[k]}(J_M) = \sum_{1 \leq i_1 < i_2 < \dots < i_k < 4} \begin{vmatrix} a_{i_1 i_1} & \dots & a_{i_1 i_k} \\ \dots & \dots & \dots \\ a_{i_k i_1} & \dots & a_{i_k i_k} \end{vmatrix} \quad k = 0, 1, 2, 3, 4 \quad (54)$$

Particularly, $a_0 = 1$, $a_1 = -(a_{11} + a_{22} + a_{33} + a_{44})$, and $a_4 = \det(J_M)$. According to Routh–Hurwitz criterion, the stable solution should satisfy the following relationship:

$$\begin{cases} \xi > 0, \quad a_2 > 0, \quad a_3 > 0, \quad a_4 > 0 \\ a_3(a_1 a_2 - a_3) - a_1^2 a_4 > 0 \end{cases} \quad (55)$$

In addition, due to the geometric constraint of the stator, the amplitude of the rotor whirling motion is limited in the range of 0 to the average air gap. $|z| = 1$ denotes the contact of the rotor and stator. The stable solution should satisfy the geometric constraint

$$|z| \leq 1 \quad (56)$$

The solution with the non-dimensional amplitude larger than 1 cannot really occur; therefore, it can

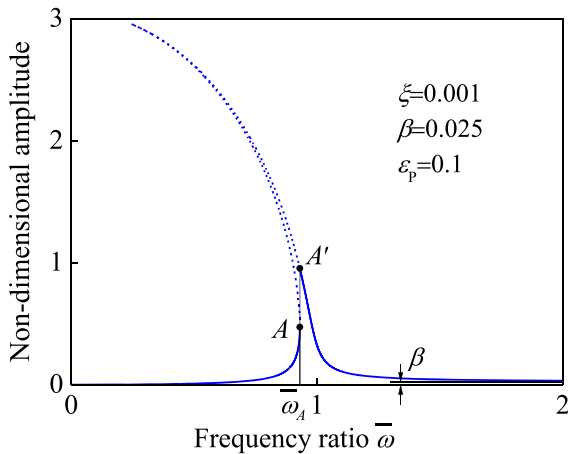


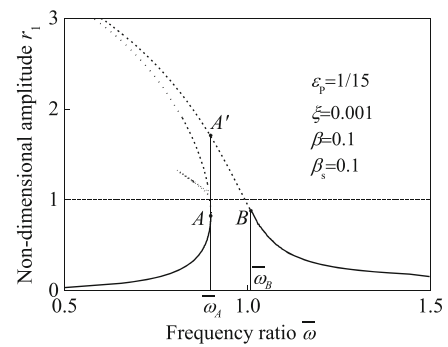
Fig. 7 Amplitude–frequency curve without static eccentricity

be included in the group of unstable solutions. As shown in Figs. 7 and 8a, both upper branches are stable according to Routh–Hurwitz criterion. However, in these branches, the solutions with amplitude $|z| > 1$ cannot be realized, so they are plotted with dashed lines that are shown in the curves of the forward whirling motion and the backward whirling motion (Figs. 7, 8). A similar situation can be observed in Figs. 9, 10, 11 and 12. Therefore, in this paper, the solutions with amplitudes larger than 1 are plotted with dashed lines.

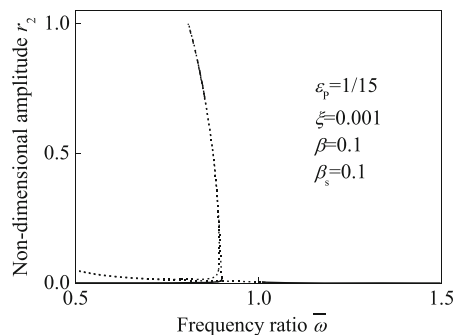
Both Eqs. (55) and (56) form the stability condition. The former is obtained by Routh–Hurwitz criterion, and it depends on the natural characteristics and reflects the stability mechanism of the system, whereas the latter provides the geometric constraint that limits the region of the rotor whirl.

4.2.3 Comparison of the degenerate model and the model by harmonic balance method

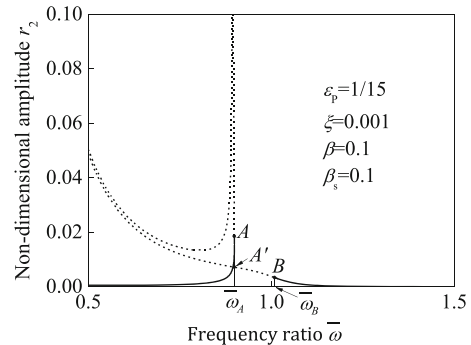
Neglecting the static eccentricity, i.e., $r_0 = 0$, we can obtain $r_2 = 0$ from the third formula in Eq. (51) when the rotor system is in steady state. Therefore, at this time, the excitation that is only caused by mass imbalance which includes a single frequency (angular speed) leads to a synchronous whirling motion with the same frequency as that of the excitation, the backward whirling motion vanishes, and the degenerate form of Eq. (52) is



(a) r_1 - $\bar{\omega}$ curve (forward whirling motion)



(b) r_2 - $\bar{\omega}$ curve (backward whirling motion)



(c) r_2 - $\bar{\omega}$ curve (backward whirling motion)

Fig. 8 Amplitude–frequency curves of the forward whirling and backward whirling motions. To clearly show the results, **c** locally displays the curve of **(b)**

$$(r_1^2 - \beta^2)\bar{\omega}^4 + \left[4\xi^2 - 2 \left(1 - \alpha - \frac{3\alpha}{2} r_1^2 \right) \right] r_1^2 \bar{\omega}^2 + \left(1 - \alpha - \frac{3\alpha}{2} r_1^2 \right)^2 r_1^2 = 0 \tag{57}$$

We can further derive the phase characteristics

$$\tan \theta_1 = \frac{-2\xi\bar{\omega}}{1 - \alpha - \frac{3\alpha r_1^2}{2} - \bar{\omega}^2} \tag{58}$$

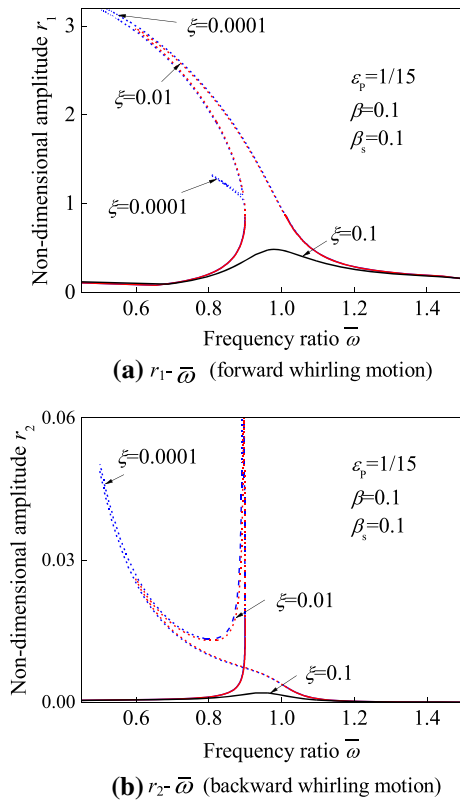


Fig. 9 Influence of the damping ratio ξ on amplitude–frequency characteristics

The results by multi-scale method coincide with those by harmonic balance method in comparisons of Eqs. (30) and (57)–(58). Therefore, the two methods have consistency. However, multi-scale method can simply address the common case of the combination of mass imbalance and static eccentricity.

4.2.4 Results and discussion

For a given frequency ratio, the solution of Eq. (52) can be obtained, and the amplitude–frequency characteristics are shown in Figs. 7 and 8. As shown in Fig. 7, the amplitude–frequency curve without static eccentricity bends to the left, and hence, the system reveals a soft type. From Eq. (30), the curve has the asymptote $\varepsilon = \beta$ as the frequency ratio $\bar{\omega}$ increases. This is the so-called self-centering. The jump phenomenon occurs when the frequency ratio slowly increases and passes through $\bar{\omega}_A$.

For the rotor system with static eccentricity, the characteristics of forward whirling motion, as well as those

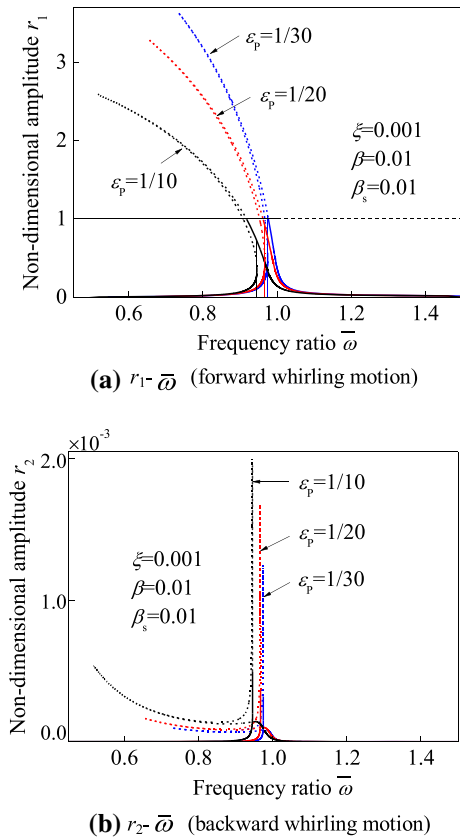


Fig. 10 Influence of the nonlinear parameter ε_p on amplitude–frequency characteristics

of the case without static eccentricity, also exhibit a softening type. However, a small branch grows from the lower branch, as shown in Fig. 8a, while the self-intersection phenomenon appears in the amplitude–frequency curve of the backward whirling motion. In general, this motion is weaker than that of the forward whirling motion, as shown in Fig. 8b, c.

According to Eq. (55), the upper branch of the amplitude–frequency curve of the forward whirling motion is stable. However, the geometric constraint in Eq. (56) results in the upper branch having one part that cannot occur (Fig. 8a). When the frequency ratio increases slowly and reaches $\bar{\omega}_A$, the system is in a critical state, and point A is a turning point. Any increment of the frequency ratio can lead to the jump phenomenon; however, the response cannot spontaneously jump from point A to point A' due to the geometric constraint of the rotor system. At this time, contact of the rotor and stator occurs, and thus, the system undergoes

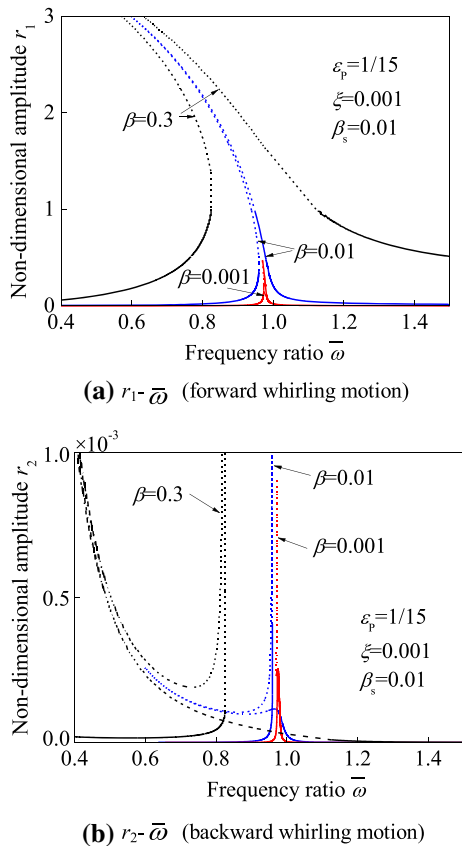


Fig. 11 Influence of the mass eccentricity ratio β on amplitude–frequency characteristics

the loss of stability. Similarly, as the frequency ratio decreases slowly and passes through $\bar{\omega}_B$, the loss of stability occurs. Therefore, in the frequency band $(\bar{\omega}_A, \bar{\omega}_B)$, the response cannot be realized and is globally unstable.

Compared with the rotor system without static eccentricity, the response of the system with static eccentricity includes the backward whirling motion in addition to the forward whirling motion. When the parameters vary, the amplitude–frequency characteristics change dramatically, which are more complex than those of the system without static eccentricity. Here, we discuss the influences of four parameters, damping ratio ξ , nonlinear parameter ε_P , mass eccentricity ratio β and static eccentricity ratio β_s , on these characteristics.

(1) Damping ratio ξ

The amplitude–frequency characteristics vary with the parameter ξ , as shown in Fig. 9. When the damping ratio increases, both amplitude–frequency curves

shorten, and the small branch growing from the lower branch of the amplitude–frequency curve of the forward whirling motion shrinks and then vanishes (Fig. 9, $\xi = 0.01$ and $\xi = 0.1$). At this time, the amplitude–frequency curve of the forward whirling motion is similar to that of the case without static eccentricity (Fig. 7). In this process, the globally unstable frequency band narrows and finally disappears. For a comparatively large damping ratio, even the amplitude–frequency curves of the two whirling motions are single-valued, and the solution becomes stable in the whole frequency domain (Fig. 9, $\xi = 0.1$). However, the overlarge damping causes harm to the isolation of the vibration. In a practical system, appropriate damping is necessary for both stability and vibration isolation.

(2) Nonlinear parameter ε_P (Stiffness ratio $\alpha = 2\varepsilon_P/3$)

When the parameter ε_P increases, the system nonlinearity becomes stronger, and the bending deflection of the amplitude–frequency curve of the forward whirling motion increases (Fig. 10a) while that of the backward whirling motion lengthens and moves toward the left (Fig. 10b). The globally unstable frequency band becomes narrower and then disappears (Fig. 10, $\varepsilon_P = 1/10$ and $\varepsilon_P = 1/20$). Due to $\varepsilon_P = 3\alpha/2$, the frequency band narrows with the increase in the stiffness ratio α . Both the large electromagnetic stiffness and the small mechanical stiffness can increase α . However, the stability margin becomes smaller simultaneously.

(3) Mass eccentricity ratio β

The responses of the two whirling motions increase remarkably as the mass eccentricity ratio β increases. For a comparatively small β (Fig. 11a, $\beta = 0.001$), there is no globally unstable frequency band. However, the frequency band begins to appear as β increases. The larger the parameter β is, the wider the frequency band. In the process of the increase in β , the amplitude–frequency curve of the backward whirling motion moves toward the left (Fig. 11b). Therefore, a decrease in the mass imbalance, which is feasible, can not only obtain a smooth and quiet operation of the rotor system but also narrow the globally unstable frequency band.

(4) Static eccentricity ratio β_s

Static eccentricity spoils the cyclic symmetry of the equilibrium point of the rotor system. The dynamic characteristics as well as the static characteristics

Fig. 12 Influence of the static eccentricity ratio β_s on amplitude–frequency characteristics

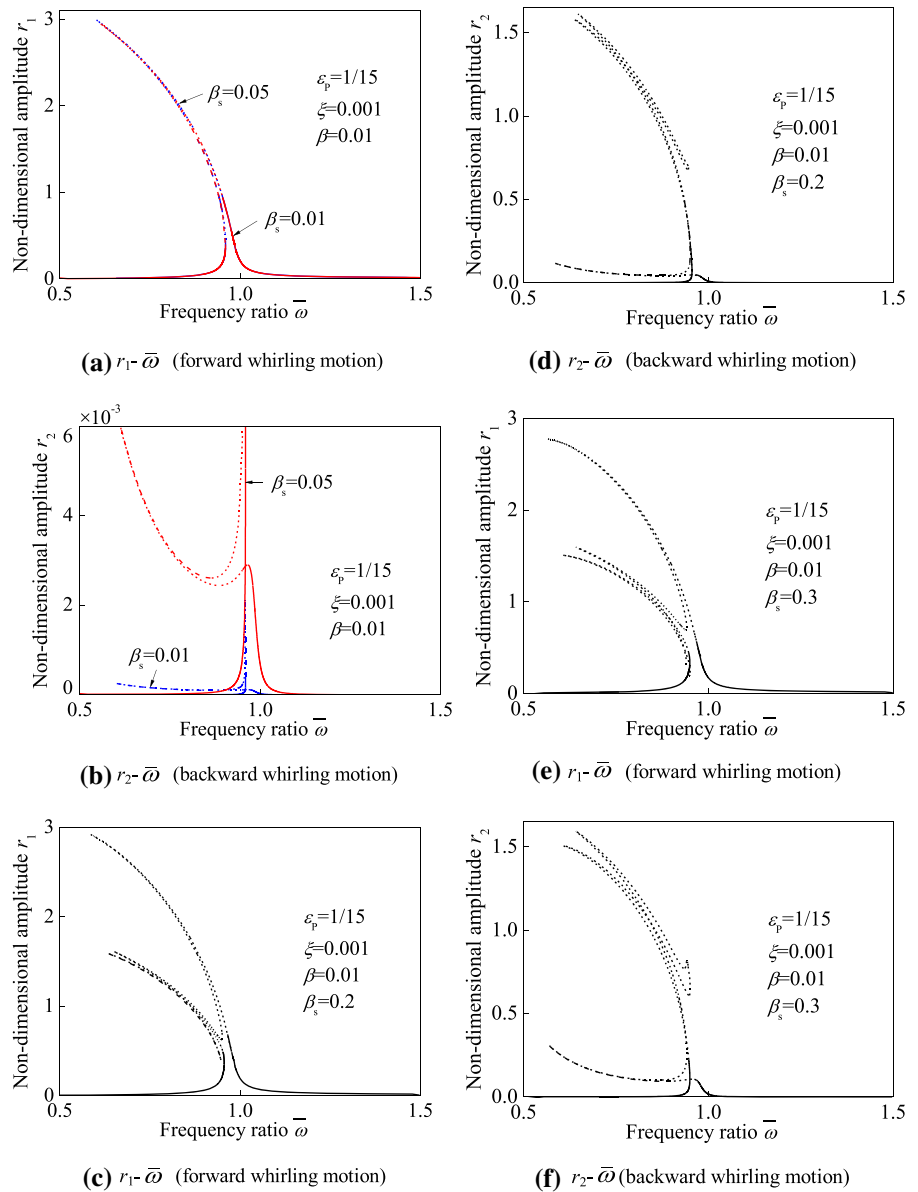


exhibit complexity, such as the small branch produced in the amplitude–frequency curve of the forward whirling motion. However, for a comparatively small static eccentricity, this curve has no small branch despite the nonlinear parameter and mass eccentricity varying in large ranges, as shown in Figs. 10a and 11a. When the static eccentricity ratio varies at a low level (Fig. 12a, b), a slight increase in the response of the forward whirling motion can be observed, and the curves corresponding to $\beta_s = 0.01$ and $\beta_s = 0.05$ almost coincide with each other (Fig. 12a). However, the curve of

the backward whirling motion lengthens dramatically (Fig. 12b).

For a comparatively large static eccentricity ratio ($\beta_s = 0.2$, Fig. 12c, d and $\beta_s = 0.3$, Fig. 12e, f), not only the forward whirling motion but also the backward whirling motion changes substantially. The small branch in the curve of the backward whirling motion as well as that of the forward whirling motion begins to appear and grows further. The two curves become more complex as the parameter β_s increases. The self-intersection phenomenon can also be observed

in the amplitude–frequency curve of the forward whirling motion. The order of magnitude of the backward whirling motion increases significantly and even matches that of the forward whirling motion. With the increase in β_s , the globally unstable frequency band appears and becomes wider. Accordingly, a decrease in the static eccentricity is another option that can narrow and even eliminate the globally unstable frequency band. Furthermore, it can also reduce the vibration and noise of the rotor system.

Next, the approximate analytical solution in Eq. (46) obtained by multi-scale method is validated by numerical simulation. Using Runge–Kutta method to solve Eq. (5), the numerical solution is carried out and can be compared with the analysis by multi-scale method. The comparisons of the calculations using various combinations of the system parameters reveal that the results obtained by the two methods agree well in the vicinity of ω_g (the natural frequency of the generating system). Here, we select the parameters $\varepsilon_p = 1/15$, $\xi = 0.1$, $\beta = 0.1$, $\beta_s = 0.1$ and $\theta_s = \pi/4$ to illustrate the comparison of the analytical solution in Eq. (46) with the numerical results, as shown in Figs. 13 and 14. The orbits, amplitudes and initial phases of the two motions are plotted in (a), (b) and (c) of the two figures, respectively. For the different detuning parameters, the orbits of the analytical solution by multi-scale method are in good agreement with those by the numerical method. From (b–c) of Figs. 13 and 14, we can see that both the amplitudes and initial phases are time-invariant when the rotor system is in steady state. Note that the results coincide with not only the assumption of the time-invariant amplitudes but also the analysis result in Eq. (50). Compared with the forward whirling motion, the backward whirling motion is comparatively weak, and the corresponding amplitude curves almost coincide with each other in Figs. 13b and 14b.

From the results, the orbits obtained by the analytical solution match well with those obtained by the numerical simulation when the detuning parameter σ_1 is close to 0, which means that the frequency ratio is in the vicinity of ω_g . As σ_1 further deviates from 0, the error between the two results increases. Moreover, the error for lower frequency ($\sigma_1 < 0$) is larger than that for higher frequency ($\sigma_1 > 0$), as shown in Figs. 13a and 14a. From Eq. (40) obtained by multi-scale method, the response caused by static eccentricity is inversely proportional to $\bar{\omega}^2$. Therefore, as

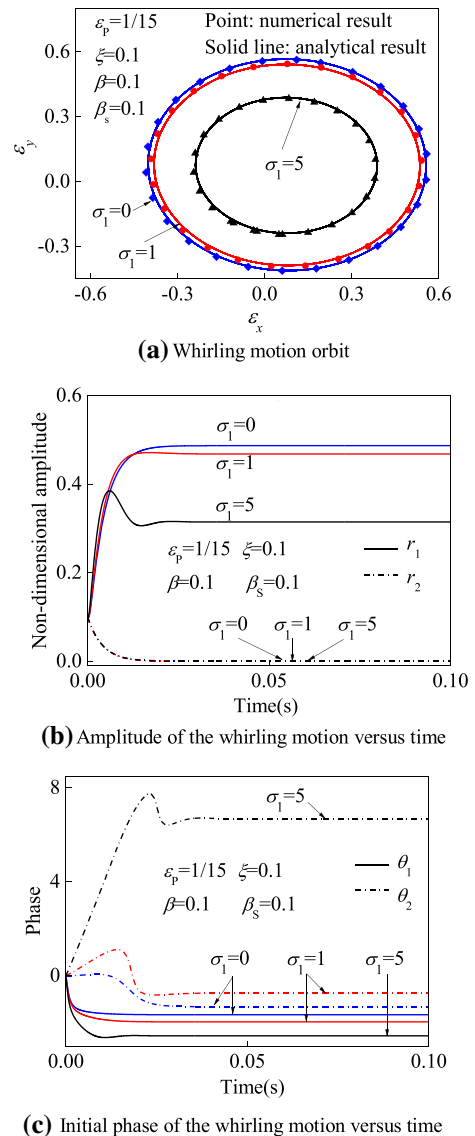


Fig. 13 Comparison of calculation results ($\sigma_1 \geq 0$)

the frequency ratio decreases, the response becomes more substantial, which leads to deviations between the orbits obtained by the analytical solution and numerical solution. However, the shapes of the orbits obtained by the two methods are similar to each other. This result denotes that the direct component depends on the frequency ratio, and multi-scale method cannot predict the response for the case when the frequency ratio is close to 0. However, we can obtain a satisfying result in the vicinity of ω_g .

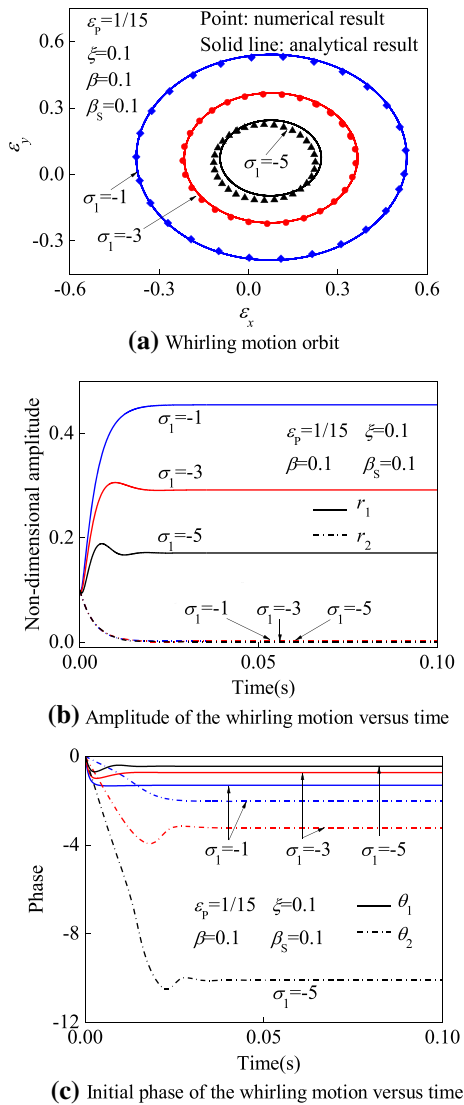


Fig. 14 Comparison of calculation results ($\sigma_1 < 0$)

5 Conclusions

This paper mainly focuses on the nonlinear characteristics of the unbalanced rotor of PMSMs in EVs and HEVs influenced by static eccentricity. Based on the effect of static eccentricity on the conservative force, the equilibrium points are carried out, and their stabilities are determined. Then, the static bifurcation of the rotor system is investigated. The frequency characteristics are studied by multi-scale method and then

validated by a numerical method. The conclusions are summarized as follows:

The static eccentricity spoils the symmetry of the system equilibrium points and results in a generic bifurcation with a defect that provides two stability conditions. One is the stiffness condition in which the electromagnetic stiffness without the relative eccentricity between the rotor and stator is less than the mechanical stiffness; the other is the eccentricity condition in which the static eccentricity of the system is less than the equivalent deformation produced by the extremum of the system conservative force without static eccentricity applied to the rotor shaft. However, this parameter has no influence on the system radial stiffness.

For the rotor system in steady state, an assumption of the time-invariant amplitudes of the forward and backward whirling motions is adopted, whereas that of the time-invariant phases is discarded. The analyses of the frequency characteristics of the main resonance by multi-scale method based on this assumption agree well with the results of the numerical method. This result shows that the assumption and the analysis are reasonable.

The response of the rotor system with mass imbalance without static eccentricity only includes the component of forward whirling motion. However, when static eccentricity is introduced, the backward whirling motion is induced in addition to the forward whirling motion. Furthermore, the two whirling modes are coupled with each other due to the nonlinearity of UMP. The backward whirling motion is comparatively weak. However, it is enhanced for comparatively large electromagnetic stiffness, large mass imbalance, large static eccentricity, small mechanical stiffness and small damping. In particular, some complex branches are induced in the amplitude–frequency curves of the two motions as static eccentricity increases.

Due to the geometric constraint of the stator, the amplitude of the rotor whirling motion is limited in the range of 0 to the average air gap. This result leads to the generation of a globally unstable frequency band. This band narrows and even disappears with increases in damping and electromagnetic stiffness and decreases in mass imbalance, mechanical stiffness and static eccentricity.

Acknowledgements This work was supported by the National Natural Science Foundations of China (Grant No. U1564210, Grant No. 51775040).

Compliance with ethical standards

Conflict of interest We declared that we have no conflicts of interest to this work.

References

- Pennacchi, P., Frosini, L.: Dynamical behaviour of a three-phase generator due to unbalanced magnetic pull. *IEE Proc.-Electr. Power Appl.* **152**(6), 1389–1400 (2005)
- Smith, A.C., Dorrell, D.G.: Calculation and measurement of unbalanced magnetic pull in cage induction motors with eccentric rotors. Part 1: analytical model. *IEE Proc.-Electr. Power Appl.* **143**(3), 193–201 (1996)
- Burakov, A., Arkkio, A.: Comparison of the unbalanced magnetic pull mitigation by the parallel paths in the stator and rotor windings. *IEEE Trans. Magn.* **43**(12), 4083–4088 (2007)
- Dorrell, D.G.: Sources and characteristics of unbalanced magnetic pull in three-phase cage induction motors with axial-varying rotor eccentricity. *IEEE Trans. Ind. Appl.* **47**(1), 12–24 (2011)
- Donát, M.: Computational modelling of the unbalanced magnetic pull by finite element method. *Procedia Eng.* **48**, 83–89 (2012)
- Yang, H.D., Chen, Y.S.: Influence of radial force harmonics with low mode number on electromagnetic vibration of PMSM. *IEEE Trans. Energy Convers.* **29**(1), 38–45 (2014)
- Žarko, D., Ban, D., Vazdar, I., Jarić, V.: Calculation of unbalanced magnetic pull in a salient-pole synchronous generator using finite-element method and measured shaft orbit. *IEEE Trans. Ind. Electron.* **59**(6), 2536–2549 (2012)
- Wang, L., Cheung, R.W., Ma, Z.Y., Ruan, J.J., Peng, Y.: Finite-element analysis of unbalanced magnetic pull in a large hydro-generator under practical operations. *IEEE Trans. Magn.* **44**(6), 1558–1561 (2008)
- Han, B., Zheng, S., Liu, X.: Unbalanced magnetic pull effect on stiffness models of active magnetic bearing due to rotor eccentricity in brushless dc motor using finite element method. *Math. Probl. Eng.* **2013**(1), 147–170 (2013)
- Kawase, Y., Mimura, N., Ida, K.: 3-D electromagnetic force analysis of effects of off-center of rotor in interior permanent magnet synchronous motor. *IEEE Trans. Magn.* **36**(4), 1858–1862 (2000)
- Kim, U., Lieu, D.K.: Effects of magnetically induced vibration force in brushless permanent-magnet motors. *IEEE Trans. Magn.* **41**(6), 2164–2172 (2005)
- Lee, S.K., Kang, G.H., Jin, H.: Analysis of radial forces in 100 kW IPM machines for ship considering stator and rotor eccentricity. In: *IEEE International Conference on Power Electronics & Ecce Asia*, pp. 2457–2461 (2011)
- Dorrell, D.G.: Calculation of unbalanced magnetic pull in small cage induction motors with skewed rotors and dynamic rotor eccentricity. *IEEE Trans. Energy Convers.* **11**(3), 483–488 (1996)
- Guo, D., Chu, F., Chen, D.: The unbalanced magnetic pull and its effects on vibration in a three-phase generator with eccentric rotor. *J. Sound Vib.* **254**, 297–312 (2002)
- Perers, R., Lundin, U., Leijon, M.: Saturation effects on unbalanced magnetic pull in a hydroelectric generator with an eccentric rotor. *IEEE Trans. Magn.* **43**(10), 3884–3890 (2007)
- Callecharan, Y., Aidanpää, J.-O.: Stability analysis of a hydropower generator subjected to unbalanced magnetic pull. *IET Sci. Meas. Technol.* **5**, 231–243 (2011)
- Ebrahimi, B.M., Javan Roshtkhari, M., Faiz, J., Khatami, S.V.: Advanced eccentricity fault recognition in permanent magnet synchronous motors using stator current signature analysis. *IEEE Trans. Ind. Electron.* **61**(4), 2041–2052 (2014)
- Ghoggal, A., Zouzou, S.E., Razik, H., Sahraoui, M., Khez-zar, A.: An improved model of induction motors for diagnosis purposes-slot skewing effect and air-gap eccentricity faults. *Energy Convers. Manage* **50**(5), 1336–1347 (2009)
- Ebrahimi, B.M., Faiz, J.: Configuration impacts on eccentricity fault detection in permanent magnet synchronous motors. *IEEE Trans. Magn.* **48**(2), 903–906 (2012)
- Ebrahimi, B.M., Roshtkhari, M.J., Faiz, J., Khatami, S.V.: Advanced eccentricity fault recognition in permanent magnet synchronous motors using stator current signature analysis. *IEEE Trans. Ind. Electron.* **61**(4), 2041–2052 (2014)
- Roux, W.L., Harley, R.G., Habetler, T.G.: Detecting rotor faults in low power permanent magnet synchronous machines. *IEEE Trans. Power Electron.* **22**(1), 322–328 (2007)
- Ebrahimi, B.M., Faiz, J., Roshtkhari, M.J., Nejjad, A.Z.: Static eccentricity fault diagnosis in permanent magnet synchronous motor using time stepping finite element method. *IEEE Trans. Magn.* **44**(11), 4297–4300 (2008)
- Ebrahimi, B.M., Faiz, J., Roshtkhari, M.J.: Static-, dynamic-, and mixed-eccentricity fault diagnoses in permanent-magnet synchronous motors. *IEEE Trans. Ind. Electron.* **56**(11), 4727–4739 (2009)
- Ebrahimi, B.M., Faiz, J.: Diagnosis and performance analysis of three-phase permanent magnet synchronous motors with static, dynamic and mixed eccentricity. *IET Electr. Power Appl.* **4**(1), 53–66 (2010)
- Ebrahimi, B.M., Faiz, J.: Magnetic field and vibration monitoring in permanent magnet synchronous motors under eccentricity fault. *IET Electr. Power Appl.* **6**(1), 35–45 (2012)
- Akar, M., Taşkin, S., Şeker, S., Çankaya, İ.: Detection of static eccentricity for permanent magnet synchronous motors using the coherence analysis. *Turk. J. Electr. Eng. Comput. Sci.* **18**(6), 963–974 (2010)
- Akar, M., Hekim, M., Orban, U.: Mechanical fault detection in permanent magnet synchronous motors using equal width discretization-based probability distribution and a neural network model. *Turk. J. Electr. Eng. Comput. Sci.* **23**, 813–823 (2015)
- Mirimani, S.M., Vahedi, A., Marignetti, F., Santis, E.D.: Static eccentricity fault detection in single-stator-single-rotor axial-flux permanent-magnet machines. *IEEE Trans. Ind. Appl.* **48**(6), 1838–1845 (2012)
- Mirimani, S.M., Vahedi, A., Marignetti, F., Stefano, R.D.: An online method for static eccentricity fault detection in

- axial flux machines. *IEEE Trans. Ind. Electron.* **62**(3), 1931–1942 (2015)
30. Hong, J., Lee, S.B., Kral, C., Haumer, A.: Detection of air-gap eccentricity for permanent magnet synchronous motors based on the d-axis inductance. *IEEE Trans. Power Electron.* **27**(5), 2605–2612 (2012)
 31. Da, Y., Shi, X.D., Krishnamurthy, M.: A new approach to fault diagnostics for permanent magnet synchronous machines using electromagnetic signature analysis. *IEEE Trans. Power Electron.* **28**(8), 4104–4112 (2013)
 32. Karami, M., Mariun, N., Mehrjou, M.R., Ab Kadir, M.Z.A., Misron, N., Radzi, M.A.M.: Static eccentricity fault recognition in three-phase line start permanent magnet synchronous motor using finite element method. *Math. Probl. Eng.* **2014**, 1–12 (2014)
 33. Huang, Y.K., Guo, B.C., Hemeida, A., Sergeant, P.: Analytical modeling of static eccentricities in axial flux permanent-magnet machines with concentrated windings. *Energies* **9**(11), 1–19 (2016)
 34. Goktas, T., Zafarani, M., Akin, B.: Discernment of broken magnet and static eccentricity faults in permanent magnet synchronous motors. *IEEE Trans. Energy Convers.* **31**(2), 578–587 (2016)
 35. Naderi, P., Fallahi, F.: Eccentricity fault diagnosis in three-phase-wound-rotor induction machine using numerical discrete modeling method. *Int. J. Numer. Model.-Electron. Netw. Devices Fields* **29**(5), 982–997 (2016)
 36. Naderi, P.: Torque/current spectral analysis for healthy and eccentricity faulty synchronous reluctance machine using mathematical modeling method. *Int. Trans. Electr. Energy Syst.* **26**(8), 1625–1645 (2016)
 37. Oumaamar, M.E., Maouche, Y., Boucherma, M., Khezzar, A.: Static air-gap eccentricity fault diagnosis using rotor slot harmonics in line neutral voltage of three-phase squirrel cage induction motor. *Mech. Syst. Signal Process.* **84**, 584–597 (2017)
 38. Kim, T.J., Hwang, S.M., Park, N.G.: Analysis of vibration for permanent magnet motors considering mechanical and magnetic coupling effects. *IEEE Trans. Magn.* **36**(4), 1346–1350 (2000)
 39. He, G.H., Huang, Z.Y., Qin, R., Chen, D.Y.: Numerical prediction of electromagnetic vibration and noise of permanent-magnet direct current commutator motors with rotor eccentricities and glue effects. *IEEE Trans. Magn.* **48**(5), 1924–1931 (2012)
 40. Shin, H.J., Choi, J.Y., Park, H.I., Jang, S.M.: Vibration analysis and measurements through prediction of electromagnetic vibration sources of permanent magnet synchronous motor based on analytical magnetic field calculations. *IEEE Trans. Magn.* **48**(11), 4216–4219 (2012)
 41. Xu, Y., Li, Z.H.: Computational model for investigating the influence of unbalanced magnetic pull on the radial vibration of large hydro-turbine generators. *J. Vib. Acoust.-Trans. ASME* **134**(5), 1–9 (2012)
 42. Wu, B.S., Sun, W.P., Li, Z.G., Li, Z.H.: Circular whirling and stability due to unbalanced magnetic pull and eccentric force. *J. Sound Vib.* **330**(21), 4949–4954 (2011)
 43. Lundström, N.L.P., Aidanpää, J.O.: Dynamic consequences of electromagnetic pull due to deviations in generator shape. *J. Sound Vib.* **301**(1–2), 207–225 (2007)
 44. Xiang, C.L., Liu, F., Liu, H., Han, L.J., Zhang, X.: Nonlinear dynamic behaviors of permanent magnet synchronous motors in electric vehicles caused by unbalanced magnetic pull. *J. Sound Vib.* **371**, 277–294 (2016)
 45. Xu, X.P., Han, Q.K., Chu, F.L.: Nonlinear vibration of a generator rotor with unbalanced magnetic pull considering both dynamic and static eccentricities. *Arch. App. Mech.* **86**(8), 1521–1536 (2016)

Publisher's Note Springer Nature remains neutral with regard to jurisdictional claims in published maps and institutional affiliations.